



This is a repository copy of *High-efficiency spray-coated perovskite solar cells utilizing vacuum-assisted solution processing*.

White Rose Research Online URL for this paper:
<http://eprints.whiterose.ac.uk/142025/>

Version: Accepted Version

Article:

Bishop, J.E., Smith, J.A. orcid.org/0000-0001-6889-4408, Greenland, C. et al. (7 more authors) (2018) High-efficiency spray-coated perovskite solar cells utilizing vacuum-assisted solution processing. *ACS Applied Materials and Interfaces*, 10 (46). pp. 39428-39434. ISSN 1944-8244

<https://doi.org/10.1021/acsami.8b14859>

This document is the Accepted Manuscript version of a Published Work that appeared in final form in *ACS Applied Materials and Interfaces*, copyright © American Chemical Society after peer review and technical editing by the publisher. To access the final edited and published work see <https://doi.org/10.1021/acsami.8b14859>

Reuse

Items deposited in White Rose Research Online are protected by copyright, with all rights reserved unless indicated otherwise. They may be downloaded and/or printed for private study, or other acts as permitted by national copyright laws. The publisher or other rights holders may allow further reproduction and re-use of the full text version. This is indicated by the licence information on the White Rose Research Online record for the item.

Takedown

If you consider content in White Rose Research Online to be in breach of UK law, please notify us by emailing eprints@whiterose.ac.uk including the URL of the record and the reason for the withdrawal request.



eprints@whiterose.ac.uk
<https://eprints.whiterose.ac.uk/>

This document is confidential and is proprietary to the American Chemical Society and its authors. Do not copy or disclose without written permission. If you have received this item in error, notify the sender and delete all copies.

High Efficiency Spray-Coated Perovskite Solar Cells Utilising Vacuum Assisted Solution Processing

Journal:	<i>ACS Applied Materials & Interfaces</i>
Manuscript ID	am-2018-14859f.R2
Manuscript Type:	Letter
Date Submitted by the Author:	n/a
Complete List of Authors:	Bishop, James; University of Sheffield, Physics and Astronomy Smith, Joel; University of Sheffield, Physics and Astronomy Greenland, Claire; The University of Sheffield, Physics and Astronomy Kumar, Vikas; University of Sheffield, Materials science and engineering Vaenas, Naoum; University of Sheffield, Physics and Astronomy Game, Onkar; University of Sheffield Department of Physics and Astronomy, Routledge, Thomas; The University of Sheffield, Physics and Astronomy Wong-Stringer, Michael; University of Sheffield, Physics and Astronomy Rodenburg, Cornelia; University of Sheffield, Materials science and engineering Lidzey, David; University of Sheffield, Physics and Astronomy

SCHOLARONE™
Manuscripts

High Efficiency Spray-Coated Perovskite Solar Cells Utilising Vacuum Assisted Solution Processing

James E. Bishop,[†] Joel A. Smith,[†] Claire Greenland,[†] Vikas Kumar,[‡] Naoum Vaenas,[†] Onkar S. Game,[†] Thomas J. Routledge,[†] Michael Wong-Stringer,[†] Cornelia Rodenburg,[‡] and David G. Lidzey^{*,†}

[†]*Department of Physics & Astronomy, University of Sheffield, Hicks Building, Hounsfield Road, Sheffield, S3 7RH, U.K.*

[‡]*Department of Materials Science & Engineering, University of Sheffield, Mappin St, Sheffield, S1 3JD, U.K.*

E-mail: d.g.lidzey@sheffield.ac.uk

Abstract

We use ultrasonic spray-coating to fabricate caesium containing triple-cation perovskite solar cells having a power conversion efficiency up to 17.8%. Our fabrication route involves a brief exposure of the partially wet spray-cast films to a coarse-vacuum; a process that is used to control film crystallisation. We show that films that are not vacuum exposed are relatively rough and inhomogeneous, while vacuum exposed films are smooth and consist of small and densely-packed perovskite crystals. The process techniques developed here represent a step towards a scalable and industrially compatible manufacturing process capable of creating stable and high-performance perovskite solar cells.

Keywords

Perovskite Solar Cell, Ultrasonic Spray-Coating, Triple-Cation Perovskite, Low Hysteresis, Thin Film

Metal-halide perovskites are high-performance semiconductor materials that have received significant attention due to their applications in photovoltaic (PV) devices. Although initial power conversion efficiencies (PCEs) of perovskite PVs were low (3.8% in 2009¹) this has increased rapidly as a result of world-wide research effort, with the best single junction devices now having an efficiency in excess of 23% PCE.² Perovskites combine many properties that make them effective photovoltaic materials, including efficient light absorption, tuneable bandgap, high charge-carrier mobility and low non-radiative recombination rates.^{3,4} Importantly, perovskite films can be formed from solution at low temperature; a useful property for mass production of cheap, efficient solar cells using a variety of scalable deposition techniques such as slot-die coating,⁵ ink-jet printing,⁶ blade coating,⁷ and spray-coating.⁸

In order for perovskite PV to be manufacturable at high volume, it is necessary to develop practical processes that enable the fabrication of high quality, uniform thin-films. Amongst the techniques that are currently being explored to fabricate perovskite PV, spray-coating has emerged as an industrially compatible process that can coat large areas at speed. Ultrasonic spray-coating was first used to deposit a $\text{CH}_3\text{NH}_3\text{I}/\text{PbCl}_2$ precursor ink which was then used to fabricate PV devices having a maximum PCE of 11%.⁸ A number of groups have subsequently explored spray-coating to deposit perovskite materials, with a range of techniques explored. Notably Das *et al.* created spray-cast $\text{CH}_3\text{NH}_3\text{PbI}_{3-x}\text{Cl}_x$ PV devices using a compact TiO_2 and spiro-OMeTAD electron- and hole-transport layers, with an efficiency of 13% demonstrated.⁹ Tait *et al.* further improved device efficiency to 15.7% by spray-casting PV devices based on a lead acetate/ PbCl_2 precursor.¹⁰ By separately spray-coating PbI_2 and MAI in a two-step process, Huang *et al.* improved device efficiency to 16.03%¹¹. Recent work by Heo *et al.*¹² explored a process in which a substrate held at 120 °C was continually spray-coated with a DMF / GBL solution containing $\text{CH}_3\text{NH}_3\text{PbI}_{3-x}\text{Cl}_x$

1
2
3 for 2 minutes. By balancing incoming and outgoing solvent fluxes (with the outgoing flux
4 controlled via solvent composition), they created a solvent-rich layer in which the growth of
5 large perovskite grains was encouraged, forming highly uniform perovskite films.¹² Such films
6 were then combined with other spin-cast charge-extraction layers to create a PV device with
7 18.3% PCE. While such efficiencies are very impressive, there are questions about whether
8 such a slow deposition process would be commercially scalable. Secondly, we note that
9 the $\text{CH}_3\text{NH}_3\text{PbI}_{3-x}\text{Cl}_x$ perovskite is thermally unstable above 85 °C due to the low energy
10 required to liberate organic decomposition products from the perovskite crystal lattice;^{13,14}
11 a feature that might limit its possible applications.
12
13
14
15
16
17
18
19
20

21 To circumvent this problem researchers have increasingly turned to the use of mixed
22 cation/halide systems. Here, formamidinium ($\text{HC}(\text{NH}_2)_2$) was first introduced into a methy-
23 lammonium based perovskite to reduce the semiconductor bandgap and thereby increase
24 optical absorption at longer wavelengths.¹⁵ It was then found that the photoactive black
25 phase of FAPbI_3 ¹⁶ could be stabilised by combining MAPbBr_3 with FAPbI_3 . Further im-
26 provements in material properties then resulted from the addition of caesium to the per-
27 ovskite, creating high-performance and stable “triple-cation” devices with PCEs of up to
28 21.1%.¹⁷ While this material system currently represents the state-of-the-art for perovskite
29 semiconductors, triple-cation perovskites have not yet been deposited by spray-coating.
30
31
32
33
34
35
36
37
38

39 In this article we demonstrate for the first time the spray-deposition of triple-cation per-
40 ovskite layers, which we then use to produce cells with PCEs up to 17.8%. Importantly,
41 we utilise a vacuum flash assisted solution processing (VASP) method¹⁸ to control the crys-
42 tallisation of the wet precursor film, with this technique allowing us to spray-coat highly
43 specular perovskite films of comparable quality to those produced via spin coating. This
44 combination of advanced materials-selection, scalable-deposition processes and control over
45 crystallisation processes are likely to be key ingredients in a spray-based manufacture process.
46
47
48
49
50
51
52

53 The perovskite precursor inks from which we have fabricated PV devices were created
54 from a mixture of caesium iodide, formamidinium iodide, lead iodide, methylammonium bro-
55
56
57
58
59
60

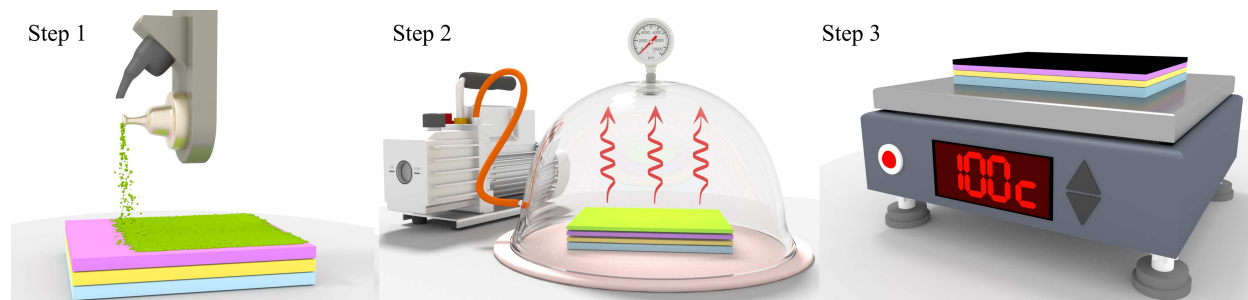


Figure 1: *Schematic illustration of the spray-deposition and VASP treatment process used to fabricate high quality perovskite films. In step 1 the spray-head moves across the surface depositing the precursor ink which then forms into a wet film. In step 2 the wet film is exposed to a partial vacuum for 5 minutes to drive out DMF from the film, forming a partially crystallised layer. In step 3 the semi-crystallised perovskite film is annealed at 100° C to form the perovskite phase.*

midate and lead bromide dissolved in a mixture of DMF and DMSO at a 4:1 ratio. The powders were mixed stoichiometrically such that the final perovskite precursor had the composition $\text{CsI}_{0.05}((\text{FAPbI}_3)_{0.85}(\text{MAPbBr}_3)_{0.15})_{0.95}$. A detailed process recipe and further experimental details are given in the Supporting Information.

Thin-films were spray-cast using a Sonotek Exactacoat system fitted with an “Impact” ultrasonic nozzle, with the system located inside a nitrogen filled glovebox. Our deposition process is summarised schematically in Figure 1. The ultrasonic spray-coating process is based upon a piezo-electric nozzle that is resonated at kHz frequency. A solution of interest is then fed through the nozzle, with shear forces created by the oscillation causing the solution to break into a mist of micron-sized droplets. A carrier gas (in this case nitrogen) is then used to guide the droplets to the surface. The key advantage of ultrasonic spray-coating over traditional air-brush techniques is that a highly uniform size distribution of droplets can be generated. This can - in principle - lead to the formation of more uniform surface coatings and hence better quality films.^{8,19,20}

In the experiments described, the ultrasonic spray-head was mounted onto a motorised gantry, with the spray-head moving across the substrate and coating it in a single pass that took a few seconds. This process reproduces the action of a R2R production line, in which a substrate moves continuously through the system (here corresponding to a coating velocity

1
2
3 of 50 mm s⁻¹).
4

5 We have found through careful optimisation that uniform perovskite precursor films can
6 be created by spray-coating the precursor ink onto a substrate held at 40 °C at a flow rate of 1
7 mL min⁻¹. Coating was performed at a spray-head velocity of 50 mm s⁻¹ with a head height
8 of 10 cm above the substrate, with a shaping gas pressure of 3 psi and an ultrasonic nozzle
9 power of 2 W. This produces a spray-pattern 3 cm wide that we use to coat our substrates
10 in a single pass. After 30 seconds, droplets were observed to have merged into a uniform wet
11 film. As we describe below it is critical that this wet film is exposed to a partial vacuum.
12 Following this VASP process, films were annealed at 100°C for 30 minutes to remove any
13 remaining DMSO and convert the film into a smooth (root mean square roughness 22 nm),
14 black perovskite film (see Figure S1).
15
16
17
18
19
20
21
22
23
24

25 To create PV devices, we have used the architecture ITO/np-SnO₂/perovskite/spiro-
26 OMeTAD/Au. Here, the nanoparticle (np) SnO₂ film²¹ was deposited by spin-coating a
27 commercially available np-SnO₂ solution onto the ITO, which was then annealed at 150°C
28 for 30 minutes. In order to complete the device, a layer of doped spiro-OMeTAD was
29 spin-cast onto the perovskite layer, followed by a gold top contact deposited by thermal
30 evaporation through a shadow-mask, forming a series of 2 mm x 2 mm electrode-contacts.
31 Devices were then tested via current-voltage (JV) measurements following exposure (through
32 a 2.6 mm² aperture mask) to light from an AM 1.5 calibrated solar simulator. To explore film
33 morphology and crystallinity, we performed scanning electron microscopy and thin-film x-
34 ray diffraction. Device homogeneity was also characterised using laser-beam-induced current
35 (LBIC) measurements. Here light from a 635 nm laser was focussed onto the cell and then
36 raster scanned in two dimensions whilst recording the photocurrent generated.
37
38
39
40
41
42
43
44
45
46
47
48

49 We have also performed time-resolved photoluminescence (TRPL) mapping of spray-cast
50 films deposited on glass. Here a pulsed laser was focused onto the film using a microscope
51 lens, with the laser spot raster scanned across the surface. The PL emission generated was
52 collected using the same microscope lens, with a time correlated single photon counting
53
54
55
56
57
58
59
60

1
2
3 technique then used to produce a TRPL decay curve at each location. These decay curves
4 were fitted with a bi-exponential function, allowing us to build an image of the bimolecular
5 recombination lifetime.
6
7

8
9 Perovskite films are polycrystalline in nature and controlling the morphology of such films
10 often presents a challenge, as the size, shape and interconnectedness of the crystal grains is
11 highly dependent on processing conditions. When triple-cation perovskite precursor films are
12 deposited by spin-coating, it is common to utilise a so-called “anti-solvent quenching tech-
13 nique”, where the precursor film is exposed to either chlorobenzene, toluene or some other
14 non-polar solvent.²² This exposure rapidly drives DMF out of the film,²³ with the remaining
15 DMSO forming a crystalline intermediary phase with the perovskite constituents.²⁴ Subse-
16 quent annealing of the film removes the DMSO, thereby forming a high quality perovskite
17 layer. In our experiments, we have found that it is relatively straightforward to create a
18 uniform triple-cation perovskite precursor film by spray-coating, however the conversion of
19 such a film into an optically dense, specular perovskite film is difficult. Simply annealing the
20 unconverted precursor-film results in perovskite-films that are characterised by poor surface
21 coverage and a high degree of roughness (100 nm). This appears to occur because there
22 are insufficient nucleation sites for the crystallisation of the perovskite phase,²⁵ and as the
23 substrate is heated, the rate of crystal growth suppresses the formation of further nucleation
24 sites. This results in a film characterised by large crystallites having a lateral size of tens of
25 microns,^{8,26} rather than a uniform film composed of small, densely-packed crystallites (see
26 Figures S2 and S3). We have found that PV devices based on triple-cation films created
27 via a regular spray-coating process followed by thermal annealing are characterised by a low
28 open circuit voltage and thus relatively low PCEs of around 10% (see Figure S4).
29
30
31
32
33
34
35
36
37
38
39
40
41
42
43
44
45
46
47
48

49 We note that Ulicna *et al.* have recently demonstrated high efficiency (17.3%) $\text{CH}_3\text{NH}_3\text{PbI}_{3-x}\text{Cl}_x$
50 spray-cast devices created by dipping a precursor film in diethyl ether to rapidly extract DMF
51 from the film.²⁷ We have tried to replicate such an anti-solvent quench process, with both
52 the perovskite-precursor and the antisolvent (chlorobenzene) delivered to the surface via
53
54
55
56
57
58
59
60

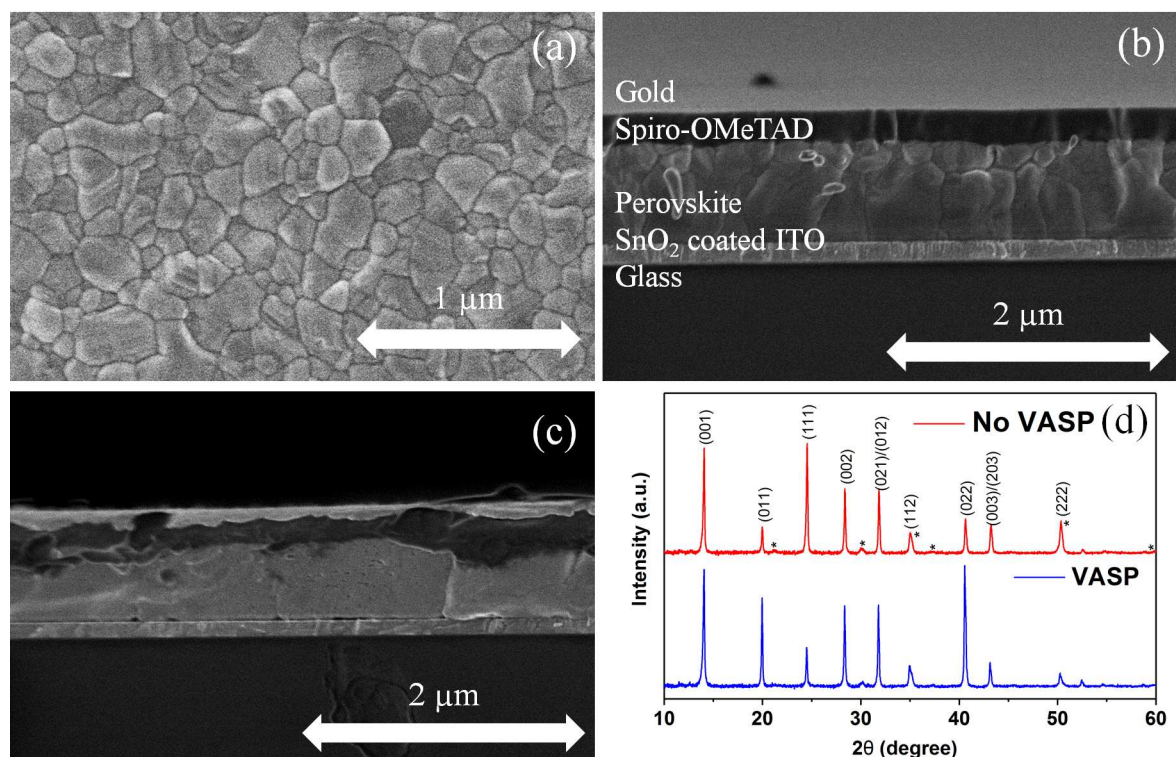


Figure 2: Part (a) shows a SEM surface image of a spray-cast VASP treated triple-cation perovskite film. Parts (b) and (c) shows a cross-sectional SEM of a completed device containing a spray-cast triple-cation perovskite layer. Here the perovskite film shown in part (b) was exposed to a vacuum, while the film shown in part (c) was thermally annealed. Part (d) shows the results of thin film XRD measurements on VASP treated and untreated films. The asterisks refer to background peaks from the substrate.

spray-coating. Unfortunately this has proved to be an ineffective means of inducing the intermediate perovskite-DMSO phase. We also note that the scalability of this process is sub-optimal, as it requires the use and recovery of significant quantities of solvent.

To address this issue, we have explored a vacuum-based solvent extraction process developed by Li *et al.*¹⁸ Here, it was shown that by exposing a freshly spin cast FA/MA mixed cation / iodide-bromide mixed anion precursor film to a low vacuum, it was possible to form a DMSO intermediary phase. On annealing such vacuum treated films, high-quality, fully-crystalline perovskite layers were formed that were used to create high efficiency (20.5%) PV devices.

We have applied this technique to freshly spray-cast triple-cation perovskite precursor

1
2
3 films, with films placed in a glovebox antechamber (reaching a final pressure of 0.8 mBar)
4 for a period of 5 minutes immediately after deposition. An SEM image of the perovskite
5 film surface and a device cross-section is shown in Figures 2a and b respectively. Here it can
6 be seen that the film is composed of tightly packed grains having an average lateral size of
7 around 200 nm. Figure 2c shows a cross-section of an otherwise identical spray-cast device
8 that was fabricated without vacuum exposure. Here, it is evident that the perovskite layer is
9 highly non-uniform, with significant thickness variations occurring over micron length-scales
10 and numerous voids visible throughout the layer.
11
12
13
14
15
16
17
18

19 To compare the crystallinity of VASP treated and annealed-only triple-cation perovskite
20 films we used X-ray diffraction (XRD) shown in Figure 2d. Samples were scanned across
21 a broad 2θ range and peaks were identified associated with the room temperature cubic
22 perovskite structure (space group $Pm3m$).²⁸ Comparing the scattering patterns of the two
23 films, we find that there is significantly lower scattering intensity from the (011) plane in the
24 untreated film, however scattering from the (111) plane is greatly increased, with scattering
25 intensity from both the (002) and (021)/(012) peaks being reduced. Notably, there is no ev-
26 idence of remnant solvent complexes or other precursor phases, which would be observed at
27 small scattering angles in the region $2\theta < 14^\circ$.²² This result suggests that the material formed
28 in both cases is a cubic perovskite, but the different crystallisation routes clearly lead to a
29 change in the crystal orientation of the resultant film. This difference in crystallographic ori-
30 entation may impact the device performance due to different charge transport characteristics
31 and interface behaviour. However the improved nanoscale morphology, controlled nucleation
32 and overall better film quality achieved via the VASP treatment route are anticipated to
33 play a dominant role in delivering high device performance.
34
35
36
37
38
39
40
41
42
43
44
45
46
47
48

49 We have utilised this vacuum treatment step to make a series of photovoltaic devices. A
50 JV curve of a champion device is shown in Figure 3a. Here, on reverse sweep, we obtained
51 a device PCE of 17.8%; a value which compares favourably to the current highest efficiency
52 spray-cast devices reported by Heo *et al.* that had an efficiency of 18.3%.¹² It is clear
53
54
55
56
57
58
59
60

that the devices have only minimal hysteresis; a fact that we attribute to the use of SnO₂ nanoparticles, which have more favourable band alignment to triple-cation perovskite than the more widely used TiO₂.^{21,29}

Table 1: *Reverse and forward sweep performance metrics for 18 spray-cast perovskite solar cells. Bold font indicates device metrics for the champion cell. Data shown in parenthesis represents average device metrics and associated standard deviation.*

Scan direction	J_{SC} (mA cm ⁻²)	V_{OC} (V)	FF (%)	PCE (%)
Forward	22.2 (21.4 ± 0.4)	1.09 (1.07 ± 0.01)	71 (65 ± 5)	17.3 (14.7 ± 1.4)
Reverse	22.3 (21.4 ± 0.4)	1.10 (1.08 ± 0.01)	73 (65 ± 4)	17.8 (15.1 ± 1.3)

In Table 1 we tabulate the average performance metrics of 18, 2.6 mm² spray-cast cells together with champion cell metrics. While this is a relatively small sample size, the low hysteresis and small standard deviation suggests our process is highly reproducible. Indeed, the J_{SC} and V_{OC} are consistently high, with variations in efficiency occurring as a result of a scatter in device fill factor (FF). The origin of this scatter in FF is currently not understood. We have determined the wavelength-dependent external quantum efficiency (EQE) of a representative cell as shown in Figure 3b. Here the integrated J_{SC} of 20.3 mA cm⁻² is within 6 % of the average value reported in Table 1 (21.4 mA cm⁻²). Unfortunately our EQE system cannot measure spectral response below 380 nm and thus the integrated J_{SC} is likely to be a slight underestimate of its actual value. We have also fabricated larger area devices (active area 16 mm²) that have similar device performance to small area devices (see Figure 3c). A stabilised measurement recorded from such a device (15.4%) is shown in Figure S5.

In order to explore the homogeneity of the device photocurrent across the active area, we have performed laser-beam induced photocurrent mapping (LBIC) on spray-cast devices fabricated either with or without the additional vacuum exposure step. Typical images are shown in Figure 4. Part (a) shows an LBIC image of a device in which the perovskite precursor material had not undergone vacuum crystallisation. Here, it can be seen that there is a significant variation in the photocurrent generation over length-scales of around

1
2
3 100 μm . Part (b) shows an image of a comparable device that was fabricated using vacuum
4 exposure; here the generated photocurrent appears significantly more uniform, apart from
5 a small number of “cold-spots” that again have an average diameter of around 100 μm . We
6 anticipate that such features most likely correspond to undissolved aggregates (most likely
7 composed of lead-based compounds) that were originally contained within the perovskite
8 precursor solution.²⁶
9
10

11
12
13
14
15 In order to understand whether charge carrier lifetimes differ between VASP treated and
16 untreated films we have performed time resolved photoluminescence (TRPL) mapping of
17 films deposited on glass substrates. Figures 4c and 4d show microscope images of regions
18 from untreated and treated samples that were then selected for mapping. It is clear from
19 these images that the VASP treated film is significantly more uniform whereas the untreated
20 film is dominated by large “flower-like” crystallites. Figures 4e and 4f show TRPL maps of
21 the long decay lifetimes extracted from fits to the bimolecular recombination decay curves.
22 Examples of the fits used to calculate these values are presented in Figure S6. Here the
23 flower-like crystallites are clearly resolved, with the emission from the edges of such features
24 apparently having much shorter lifetimes than those recorded from their centre. We speculate
25 this is due to a higher density of non-radiative recombination centres found in these regions
26 that occur as a result of a more disordered macro-structure together with compositional
27 variations that are also observed in energy-dispersive x-ray spectroscopy (see Figure S7). In
28 contrast, the VASP treated films are characterised by much longer average decay-lifetimes,
29 with such decay transients having enhanced uniformity across the film surface.
30
31
32
33
34
35
36
37
38
39
40
41
42
43
44

45 In conclusion, we have demonstrated a method to fabricate triple-cation based perovskite
46 solar cells having a peak power conversion efficiency of 17.8% using a combination of ultra-
47 sonic spray-coating and vacuum assisted solution processing. The device efficiencies demon-
48 strated are comparable with the highest efficiencies reported for a spray-cast perovskite
49 devices.¹² Here the use of a relatively coarse vacuum both removes trapped solvent and
50 initiates crystallization through controlled nucleation, with the films produced being of com-
51
52
53
54
55
56
57
58
59
60

1
2
3 parable quality to those produced via spin-coating. This allows us to create PV devices
4 having enhanced photocurrent uniformity as evidenced using photocurrent mapping studies.
5 Importantly, our work is the first example of the use of spray-casting to fabricate photovoltaic
6 devices based on a triple-cation perovskite. Such perovskite materials are compatible with
7 stable device-operation over prolonged time-scales¹⁷ and have higher efficiency than those
8 based on methylammonium lead triiodide; the current material of choice used to spray-
9 cast PV devices.⁸⁻¹² We anticipate that further process optimisation will allow us to create
10 spray-coated perovskite devices having efficiencies that match the state-of-the-art. The pro-
11 cess demonstrated uses a rapid, single-pass, spray-technique and is thus an important step
12 towards high-speed, high volume perovskite PV device manufacture. Indeed, we expect that
13 the deposition process used here could be further accelerated by using flash infrared annealing
14 instead of the relatively slow thermal-annealing stage.³⁰ We emphasize that the use of vac-
15 uum processing steps are compatible with high-volume manufacture; for example metallised
16 films are routinely deposited on moving substrate films such as polyethylene terephthalate
17 (PET) via vacuum-based physical vapour deposition (PVD).³¹ Notably, our process does not
18 require the use of large quantities of solvent either in the initial spray-deposition step or in
19 a subsequent anti-solvent quench, and is thus a step towards a more environmentally benign
20 manufacture process.
21
22
23
24
25
26
27
28
29
30
31
32
33
34
35
36
37
38
39
40

41 Acknowledgement

42
43
44 This work was funded by the UK Engineering and Physical Sciences Research Council (EP-
45 SRC) via grants EP/M025020/1 “High resolution mapping of performance and degradation
46 mechanisms in printable photovoltaic devices”, EPSRC grant EP/N008065/1 “Secondary
47 Electron Emission - Microscopy for Organics With Reliable Engineering-Properties”, and
48 EP/M014797/1 “Improved Understanding, Development and Optimization of Perovskite-
49 based Solar Cells”. We also thank the EPSRC for PhD studentships via the University of
50
51
52
53
54
55
56
57
58
59
60

1
2
3 Sheffield DTG account (J.E.B. and T.J.R.) and from the Centre for Doctoral Training in
4 New and Sustainable PV, EP/L01551X/1 (M.W.S., J.A.S. and C.G.). We thank Dave Coles
5 for providing an illustration of the spray-deposition process for figure 1.
6
7
8
9

10 11 Supporting Information Available

12
13
14 Experimental details on perovskite sample preparation and additional characterisation in-
15 cluding AFM, PL and EDX.
16

17
18 This material is available free of charge via the Internet at <http://pubs.acs.org/>.
19
20
21
22

23 Conflict of Interest

24
25
26 D.G.L. is co-director of the company Ossila Ltd that retail materials and equipment for
27 perovskite photovoltaic device research and development.
28
29
30
31

32 References

- 33
34
35
36 (1) Kojima, A.; Teshima, K.; Shirai, Y.; Miyasaka, T. Organometal Halide Perovskites
37 as Visible-Light Sensitizers for Photovoltaic Cells. *Journal of the American Chemical*
38 *Society* **2009**, *131*, 6050–6051.
39
40
41
42 (2) NREL, Best Research-Cell Efficiencies. [https://www.nrel.gov/pv/assets/images/](https://www.nrel.gov/pv/assets/images/efficiency-chart-20180716.jpg)
43 [efficiency-chart-20180716.jpg](https://www.nrel.gov/pv/assets/images/efficiency-chart-20180716.jpg), Online; accessed 15 August 2018.
44
45
46
47 (3) Stranks, S. D.; Eperon, G. E.; Grancini, G.; Menelaou, C.; Alcocer, M. J.; Leijtens, T.;
48 Herz, L. M.; Petrozza, A.; Snaith, H. J. Electron-Hole Diffusion Lengths Exceeding
49 1 Micrometer in an Organometal Trihalide Perovskite Absorber. *Science* **2013**, *342*,
50 341–344.
51
52
53
54
55
56
57
58
59
60

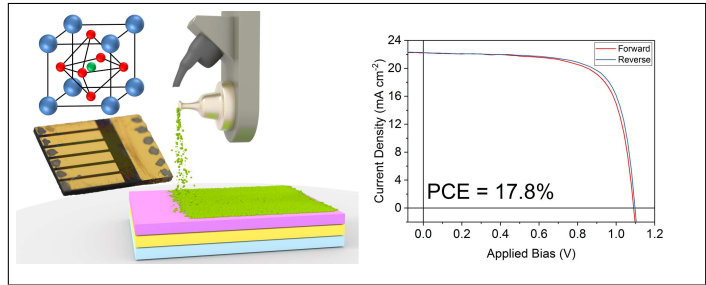
- 1
2
3 (4) Green, M. A.; Ho-Baillie, A.; Snaith, H. J. The Emergence of Perovskite Solar Cells.
4 *Nature Photonics* **2014**, *8*, 506–514.
5
6
7
8 (5) Schmidt, T. M.; Larsen-Olsen, T. T.; Carlé, J. E.; Angmo, D.; Krebs, F. C. Upscaling
9 of Perovskite Solar Cells: Fully Ambient Roll Processing of Flexible Perovskite Solar
10 Cells with Printed Back Electrodes. *Advanced Energy Materials* **2015**, *5*, 1500569.
11
12
13
14 (6) Li, S.-G.; Jiang, K.-J.; Su, M.-J.; Cui, X.-P.; Huang, J.-H.; Zhang, Q.-Q.; Zhou, X.-Q.;
15 Yang, L.-M.; Song, Y.-L. Inkjet Printing of CH₃NH₃PbI₃ on a Mesoscopic TiO₂
16 2 Film for Highly Efficient Perovskite Solar Cells. *Journal of Materials Chemistry A*
17 **2015**, *3*, 9092–9097.
18
19
20
21
22
23 (7) Deng, Y.; Peng, E.; Shao, Y.; Xiao, Z.; Dong, Q.; Huang, J. Scalable Fabrication of
24 Efficient Organolead Trihalide Perovskite Solar Cells with Doctor-Bladed Active Layers.
25 *Energy & Environmental Science* **2015**, *8*, 1544–1550.
26
27
28
29
30 (8) Barrows, A. T.; Pearson, A. J.; Kwak, C. K.; Dunbar, A. D.; Buckley, A. R.;
31 Lidzey, D. G. Efficient Planar Heterojunction Mixed-Halide Perovskite Solar Cells De-
32 posited via Spray-Deposition. *Energy & Environmental Science* **2014**, *7*, 2944–2950.
33
34
35
36
37 (9) Das, S.; Yang, B.; Gu, G.; Joshi, P. C.; Ivanov, I. N.; Rouleau, C. M.; Aytug, T.;
38 Geohegan, D. B.; Xiao, K. High-Performance Flexible Perovskite Solar Cells by using a
39 Combination of Ultrasonic Spray-Coating and Low Thermal Budget Photonic Curing.
40 *Acs Photonics* **2015**, *2*, 680–686.
41
42
43
44
45 (10) Tait, J.; Manghooli, S.; Qiu, W.; Rakocevic, L.; Kootstra, L.; Jaysankar, M.; de la
46 Huerta, C. M.; Paetzold, U. W.; Gehlhaar, R.; Cheyins, D.; Heremans, P.; Poortmans, J.
47 Rapid Composition Screening for Perovskite Photovoltaics via Concurrently Pumped
48 Ultrasonic Spray Coating. *Journal of Materials Chemistry A* **2016**, *4*, 3792–3797.
49
50
51
52
53 (11) Huang, H.; Shi, J.; Zhu, L.; Li, D.; Luo, Y.; Meng, Q. Two-Step Ultrasonic Spray
54
55
56
57
58
59
60

- 1
2
3 Deposition of CH₃NH₃PbI₃ for Efficient and Large-Area Perovskite Solar Cell.
4
5 *Nano Energy* **2016**, *27*, 352–358.
6
7
- 8 (12) Heo, J. H.; Lee, M. H.; Jang, M. H.; Im, S. H. Highly Efficient CH₃NH₃PbI_{3-x}Cl_x
9
10 Mixed Halide Perovskite Solar Cells Prepared by Re-dissolution and Crystal Grain
11
12 Growth via Spray Coating. *Journal of Materials Chemistry A* **2016**, *4*, 17636–17642.
13
14
- 15 (13) Conings, B.; Drijkoningen, J.; Gauquelin, N.; Babayigit, A.; D’Haen, J.;
16
17 D’Olieslaeger, L.; Ethirajan, A.; Verbeeck, J.; Manca, J.; Mosconi, E.; De Angelis, F.;
18
19 Boyen, H.-G. Intrinsic Thermal Instability of Methylammonium Lead Trihalide Per-
20
21 ovskite. *Advanced Energy Materials* **2015**, *5*, 1500477.
22
23
- 24 (14) Juarez-Perez, E. J.; Ono, L. K.; Maeda, M.; Jiang, Y.; Hawash, Z.; Qi, Y. Photodecom-
25
26 position and Thermal Decomposition in Methylammonium Halide Lead Perovskites and
27
28 Inferred Design Principles to Increase Photovoltaic Device Stability. *Journal of Mate-
29
30 rials Chemistry A* **2018**, *6*, 9604–9612.
31
32
- 33 (15) Pellet, N.; Gao, P.; Gregori, G.; Yang, T.-Y.; Nazeeruddin, M. K.; Maier, J.; Grätzel, M.
34
35 Mixed-Organic-Cation Perovskite Photovoltaics for Enhanced Solar-Light Harvesting.
36
37 *Angewandte Chemie* **2014**, *126*, 3215–3221.
38
39
- 40 (16) Jeon, N. J.; Noh, J. H.; Yang, W. S.; Kim, Y. C.; Ryu, S.; Seo, J.; Seok, S. I. Compo-
41
42 sitional Engineering of Perovskite Materials for High-Performance Solar Cells. *Nature*
43
44 **2015**, *517*, 476–480.
45
46
- 47 (17) Saliba, M.; Matsui, T.; Seo, J.-Y.; Domanski, K.; Correa-Baena, J.-P.; Nazeerud-
48
49 din, M. K.; Zakeeruddin, S. M.; Tress, W.; Abate, A.; Hagfeldt, A.; Grätzel, M. Cesium-
50
51 Containing Triple Cation Perovskite Solar Cells: Improved Stability, Reproducibility
52
53 and High Efficiency. *Energy & environmental science* **2016**, *9*, 1989–1997.
54
55
- 56 (18) Li, X.; Bi, D.; Yi, C.; Décoppet, J.-D.; Luo, J.; Zakeeruddin, S. M.; Hagfeldt, A.;
57
58
59
60

- Grätzel, M. A Vacuum Flash-Assisted Solution Process for High-Efficiency Large-Area Perovskite Solar Cells. *Science* **2016**, aaf8060.
- (19) Majumder, M.; Rendall, C.; Li, M.; Behabtu, N.; Eukel, J. A.; Hauge, R. H.; Schmidt, H. K.; Pasquali, M. Insights into the Physics of Spray Coating of SWNT Films. *Chemical Engineering Science* **2010**, *65*, 2000–2008.
- (20) Bishop, J. E.; Routledge, T. J.; Lidzey, D. G. Advances in Spray-Cast Perovskite Solar Cells. *The journal of physical chemistry letters* **2018**, *9*, 1977–1984.
- (21) Jiang, Q.; Zhang, L.; Wang, H.; Yang, X.; Meng, J.; Liu, H.; Yin, Z.; Wu, J.; Zhang, X.; You, J. Enhanced Electron Extraction using SnO₂ for High-Efficiency Planar-Structure HC (NH₂)₂ PbI₃-based Perovskite Solar Cells. *Nature Energy* **2017**, *2*, 16177.
- (22) Paek, S.; Schouwink, P.; Athanasopoulou, E. N.; Cho, K.; Grancini, G.; Lee, Y.; Zhang, Y.; Stellacci, F.; Nazeeruddin, M. K.; Gao, P. From Nano-to Micrometer Scale: the Role of Antisolvent Treatment on High Performance Perovskite Solar Cells. *Chemistry of Materials* **2017**, *29*, 3490–3498.
- (23) Jeon, N. J.; Noh, J. H.; Kim, Y. C.; Yang, W. S.; Ryu, S.; Seok, S. I. Solvent Engineering for High-Performance Inorganic–Organic Hybrid Perovskite Solar Cells. *Nature materials* **2014**, *13*, 897–903.
- (24) Yang, W. S.; Noh, J. H.; Jeon, N. J.; Kim, Y. C.; Ryu, S.; Seo, J.; Seok, S. I. High-Performance Photovoltaic Perovskite Layers Fabricated through Intramolecular Exchange. *Science* **2015**, *348*, 1234–1237.
- (25) Zhou, Y.; Game, O. S.; Pang, S.; Padture, N. P. Microstructures of Organometal Trihalide Perovskites for Solar Cells: their Evolution from Solutions and Characterization. *The journal of physical chemistry letters* **2015**, *6*, 4827–4839.

- 1
2
3
4 (26) Bishop, J. E.; Mohamad, D. K.; Wong-Stringer, M.; Smith, A.; Lidzey, D. G. Spray-
5 Cast Multilayer Perovskite Solar Cells with an Active-Area of 1.5 cm². *Scientific reports*
6 **2017**, *7*, 7962.
7
8
9
10 (27) Ulicna, S.; Dou, B.; Kim, D. H.; Zhu, K.; Walls, J. M.; Bowers, J. W.; van Hest, M. F.
11 Scalable Deposition of High-Efficiency Perovskite Solar Cells by Spray-Coating. *ACS*
12 *Applied Energy Materials* **2018**, *1*, 1853–1857.
13
14
15
16 (28) Jacobsson, T. J.; Correa-Baena, J.-P.; Pazoki, M.; Saliba, M.; Schenk, K.; Grätzel, M.;
17 Hagfeldt, A. Exploration of the Compositional Space for Mixed Lead Halogen Per-
18 ovskites for High Efficiency Solar Cells. *Energy & Environmental Science* **2016**, *9*,
19 1706–1724.
20
21
22
23
24
25 (29) Baena, J. P. C.; Steier, L.; Tress, W.; Saliba, M.; Neutzner, S.; Matsui, T.; Giordano, F.;
26 Jacobsson, T. J.; Kandada, A. R. S.; Zakeeruddin, S. M.; Petrozza, A.; Abate, A.;
27 Nazeerruddin, M. K.; Grätzel, M.; Hagfeldt, A. Highly Efficient Planar Perovskite
28 Solar Cells Through Band Alignment Engineering. *Energy & Environmental Science*
29 **2015**, *8*, 2928–2934.
30
31
32
33
34
35 (30) Sanchez, S.; Hua, X.; Phung, N.; Steiner, U.; Abate, A. Flash Infrared Annealing for
36 Antisolvent-Free Highly Efficient Perovskite Solar Cells. *Advanced Energy Materials*
37 **2018**, *8*, 1702915.
38
39
40
41
42 (31) Abbas, G.; Assender, H.; Ibrahim, M.; Martin Taylor, D. Organic Thin-Film Transis-
43 tors with Electron-Beam Cured and Flash Vacuum Deposited Polymeric Gate Dielec-
44 tric. *Journal of Vacuum Science & Technology B, Nanotechnology and Microelectronics:*
45 *Materials, Processing, Measurement, and Phenomena* **2011**, *29*, 052401.
46
47
48
49
50
51
52
53
54
55
56
57
58
59
60

Graphical TOC Entry



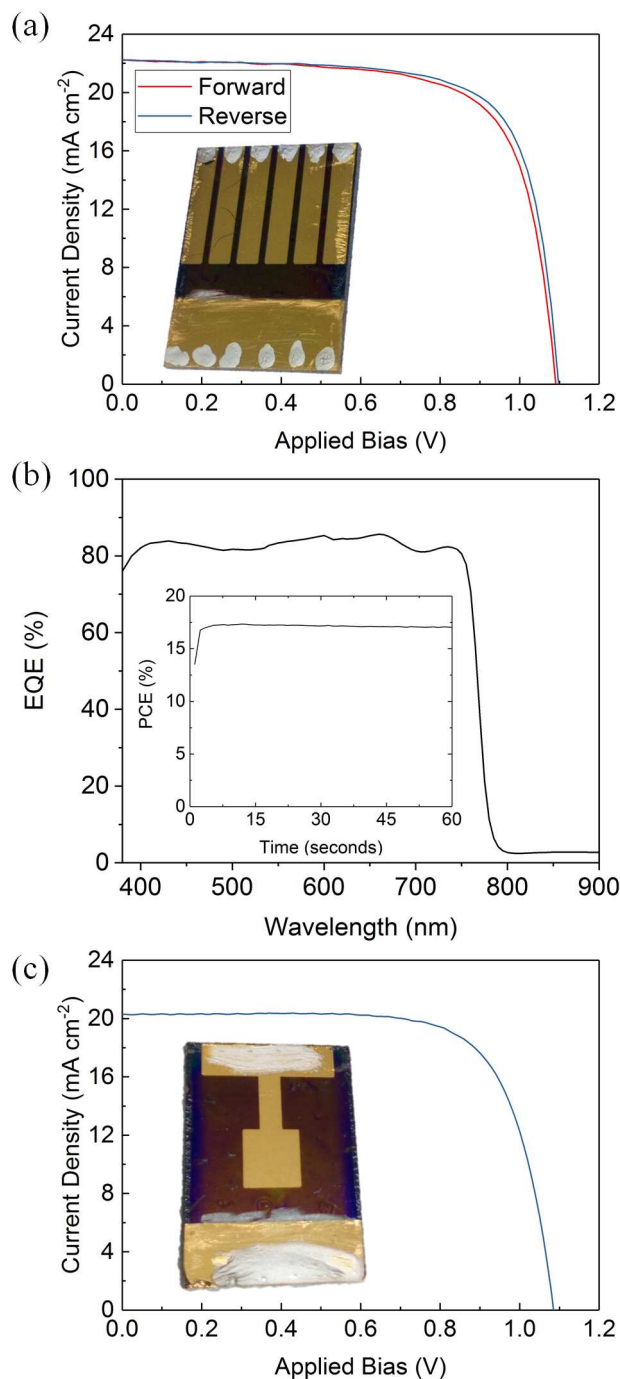


Figure 3: Part (a) shows the current voltage characteristics for the champion spray-cast triple-cation perovskite solar cell with a reverse scan efficiency of 17.8%. The inset shows a photograph of the device. Part (b) shows an EQE spectrum recorded from a representative spray-cast perovskite cell (J_{SC} 21.4 mA cm^{-2}) corresponding to an integrated current of 20.3 mA cm^{-2} . The inset shows output power of the champion device held at a fixed voltage close to the maximum power point (920 mV) recorded over 60 s indicating a stabilised power output of 17%. Part (c) shows the current voltage characteristics of a larger area device with a reverse scan efficiency of 16%. The inset shows a photograph of the device.

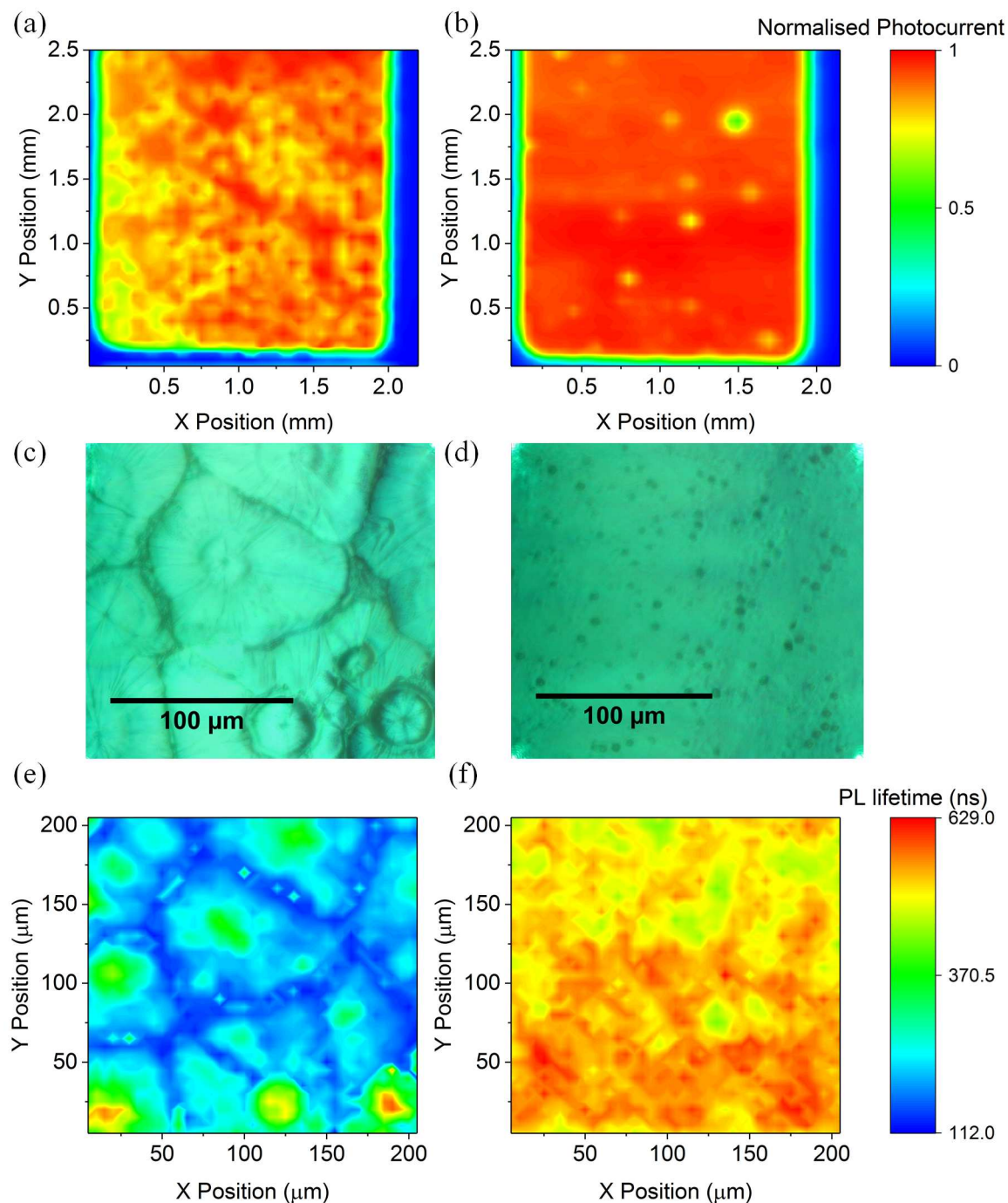


Figure 4: Laser-beam-induced current (LBIC) mapping, optical-microscope images, and time-resolved photoluminescence (TRPL) mapping of spray-cast perovskite solar cells and films. Part (a) is an LBIC image of device that includes a perovskite layer that was thermally annealed only. Part (b) is a comparable device in which the perovskite precursor film was treated using the additional VASP process. Part (c) is an optical micrograph of a spray-cast film deposited on glass that had simply been annealed, and part (d) is a film that has undergone VASP treatment. Parts (e) and (f) are TRPL maps of the same regions of the film shown in parts (c) and (d).